ELSEVIER

Cryogenics 40 (2000) 179–189

Cryogenics

www.elsevier.com/locate/cryogenics

M&M: Multi-conductor Mithrandir code for the simulation of thermal-hydraulic transients in superconducting magnets

L. Savoldi [1], R. Zanino *

Dipartimento di Energetica, Politecnico di Torino, 24, C.so Duca degli Abruzzi, 10129 Torino, Italy

Received 26 January 2000; accepted 27 April 2000

Abstract

The analysis of superconducting magnets can require the simultaneous simulation of several conductors. The multi-conductor Mithrandir (M&M) code has been developed for this purpose from the Mithrandir code (Zanino R, De Palo S, Bottura L. J Fus Energy 1995;14:25), which was used for the simulation of thermal-hydraulic transients of single two-channel cable-in-conduit conductors (CICCs) cooled by supercritical helium. The M&M code is able to describe simultaneously an arbitrary number of one- or two-channel conductors, allowing for different kinds of coupling between them, and for different topologies of the assembly. The new code has been validated in three different situations, leading to good agreement both with results obtained with Mithrandir and with experimental data.

Keywords: Cable-in-conduit conductors; Superconducting cables; Supercritical helium; Heat transfer; Fusion magnets

1. Introduction

The development of superconducting magnets for nuclear fusion, in particular within the frame of the International Thermonuclear Experimental Reactor (ITER) has significantly evolved over the last few years. The starting point, and at the same time the essential building block of most of this work, is the dual-channel cable-in-conduit conductor (CICC), see Fig. 1. The main aspects of the behavior of such a system, at the stage of the single-conductor studies, were pioneered in the quench initiation and propagation study (QUIPS) for the SMES–CICC [2]. Within the ITER framework the concept was then thoroughly investigated in 1997 in the quench experiment on long length (QUELL) [3], which was performed in the SULTAN facility at Villigen PSI, Switzerland, as a result of worldwide collaboration. At the intermediate stage towards the test of a full coil (which we consider here as a set of single conductors electrically connected in series by joints) significant additional problems and issues arise, in particular that of the joints, for which a large amount of testing studies were performed during 1998 and 1999 [4–7]. Finally, in a full coil thermal coupling between different turns, or layers, or pancakes, may be significant, depending on the time scale of the phenomena to be considered. The first tests of full coils with dual-channel CICC are planned for mid-2000 for the ITER central solenoid model coil (CSMC) [8,9] at the JAERI facility in Naka, Japan, and for the end of 2000 for the ITER toroidal field model coil (TFMC) [10,11] at the TOSKA facility of the Forschungszentrum in Karlsruhe, Germany.

In strict correlation to the above-mentioned evolution of the problems, also an evolution of the computational tools must obviously be foreseen, and in this paper we shall be particularly concerned with the tools for the prediction of the evolution of the thermal-hydraulic transients. [2] In the recent past the development of the concept of the dual-channel CICC led indeed to the

* Corresponding author. Tel.: +39-011-564-4490; fax: +39-011-564-4499.

E-mail addresses: savoldi@polito.it (L. Savoldi), zanino@polito.it (R. Zanino).

[1] Tel.: +39-011-564-4447; fax: +39-011-564-4499.

[2] For the sake of simplicity we make the assumption of uniform current density on any conductor cross-section. Many studies are being performed on the problem of current distribution in multi-strand conductors, but this issue is beyond the scope of the present paper. Notice however that the development of a model with non-uniform current distribution on the cable cross-section obviously requires the possibility to describe non-uniform *temperature* distributions over the same area, and as such also points to the need for something like a multi-conductor model, as the present one.

0011-2275/00/$ - see front matter
PII: S0011-2275(00)00027-8

Nomenclature

A	helium cross-section (m^2)
c	helium sound speed (m/s)
c_v	helium specific heat at constant volume (J/kg K)
$C_{i\leftrightarrow j}$	transport coefficient in the exchange between ith and jth conductor (see Eq. (8))
$D_{i\leftrightarrow j}$	driving term of the exchange between ith and jth conductor (see Eq. (8))
h	heat transfer coefficient (W/m^2 K)
$k_{i\leftrightarrow j}$	coupling flux between ith and jth conductor (see Eq. (8))
$\underline{\underline{K}}$	coupling matrix in the multi-conductor model
$\underline{\underline{\ell}}$	system coefficient matrix in the single-conductor model
$\underline{\underline{L}}$	system coefficient matrix in the multi-conductor model
m	iteration index
$NCOND$	number of conductors analyzed by M&M
$NODES$	number of spatial nodes on a single conductor
p	helium pressure (Pa)
Q	external heating power (W)
$S_{i\leftrightarrow j}$	exchange perimeter (m) between ith and jth conductor (see Eq. (8))
t	time (s)
T	temperature (K)
TOL	required relative accuracy in under-relaxation loop
$\underline{u}$	vector of the unknowns in the single-conductor model
$\underline{U}$	vector of the unknowns in the multi-conductor model
V	helium flow speed (m/s)
w	helium enthalpy (J/kg)
x	coordinate along the axial direction of the ith conductor, measured from helium inlet (m)

Greeks

α	under-relaxation coefficient used in the iterations (see Fig. 2)
Δt	time step (s)
ε	global error in the solution
ϕ	Gruneisen parameter
Λ_ρ	mass source (kg/m^3 s)
Λ_V	momentum source (N/m^3)
Λ_e	energy source (W/m^3)
ρ	helium density (kg/m^3)
Ω_1	first type of coupling between conductors implemented in M&M (see Table 1)
Ω_2	second type of coupling between conductors implemented in M&M (see Table 1)

Subscripts

B	bundle region
H	hole region
St	strands
Jk	jacket
in	inlet
out	outlet

development of the two-fluid code Mithrandir [1,12] from the one-fluid code Gandalf [13]. The cross-section of a dual-channel conductor is modeled by Mithrandir accounting for: (1) two fluid regions (hole and bundle) separated typically by a helical interface, (2) superconducting strands, and (3) jacket and insulation. The need for a simultaneous treatment of the external hydraulic circuit, in view of a predictive use of the same tool, led eventually to the coupling of the hydraulic solver Flower [14,15] with Mithrandir [16]. Very recently, then, the need for an adequate treatment of the joint + conductor system led to the extension of Mithrandir to a quasi 1-D model allowing variable geometrical and material properties along the hydraulic path [17]. (Here and below, by "conductor" we mean a part or the whole of a superconducting cable between two joints.)

A number of present and future problems, however, clearly indicate the inadequacy of the present tools, notwithstanding their ability to accurately reproduce experimental results in relatively controlled situations [18–20]. In particular, the need for the *simultaneous treatment of several conductors thermally and hydraulically coupled* (→ multi-conductor model) clearly arises, and will constitute the main object of the present paper. In a sense, the traditional 1-D model intrinsic to most of present-day codes needs to somehow evolve to account for the major 3-D effects in a coil, at least approximately. In the CSMC, e.g., the measurement in situ of the current-sharing temperature of the conductor will be performed using external heaters, which however cannot simultaneously heat all layers of the coil. Now, if the inter-turn and/or the inter-layer coupling time constants are not very long compared to the time scale of interest, the heat exchange between different conductors must be included in the model, and details of the thermal-hydraulic transient in "neighboring" conductors become relevant. The treatment of all neighboring conductors as parallel heated channels using Flower [14,15], i.e., accounting only for the helium but neglecting the solids and the two-channel structure may not be adequate in general. This is just one example for the need of a new tool. Another example of similar nature comes from the

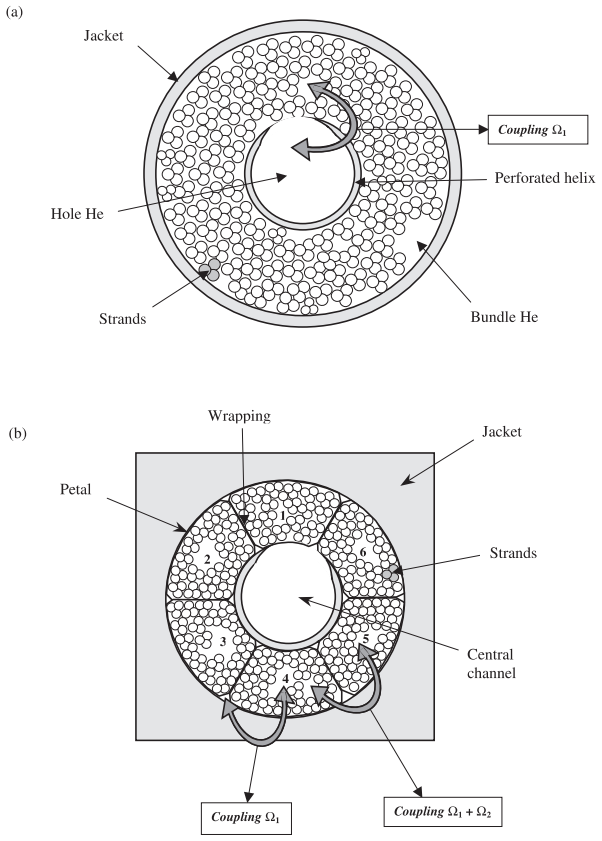

Fig. 1. Sketches of dual-channel CICC (not in scale): (a) cross-section of the QUELL conductor used in the test of artificial quench, (b) cross-section of the CSMC-like conductor used in the test of heat transfer between petals.

case of asymmetrically heated legs of a joint [6,17], which can be relevant especially in the TFMC test program and which is going to be considered in some detail below. A fancier, albeit relevant example, which will also be addressed below, comes from the consideration of the last-but-one stage of the cabling of many CICC. If a wrapping is applied at this stage, it produces petals, which effectively work as partially separate subchannels, where partially de-coupled thermal-hydraulic evolution may be possible to some extent [21].

The present paper is organized as follows: in the next section the model implemented in the M&M code is presented. The code is then validated in different situations:

1. The simulation of an artificial quench is presented for the single two-channel CICC of QUELL (see Fig. 1(a)), *treated as two coupled conductors*. This is a rather degenerate and particularly "tough" situation, in view of the very strong coupling between the two conductors, and the M&M results are compared to those obtained by Mithrandir for the same transient.
2. Heat propagation between petals is studied on a short CSMC-like conductor (see Fig. 1(b)), and the results are compared semi-quantitatively to experimental data [21].
3. Heat exchange between the two halves of a lap-type joint is studied, and the code is validated against experimental data from the stainless steel full size joint sample (SS-FSJS) [4,6].

Finally, conclusions and perspective of the present work are discussed.

2. Model description

The model implemented in M&M uses the two-fluid Mithrandir model as the essential building block for the description of the transient evolution in each conductor. After a brief review of the single-conductor model implemented in Mithrandir, the new multi-conductor model is presented.

2.1. Brief overview of the single-conductor model in Mithrandir

The model implemented in Mithrandir accounts for different thermodynamic state of the helium in the bundle region and of the helium in the central channel. The two fluids are separately modeled by a set of Euler equation [1] written in the primitive variables flow speed V, pressure p and temperature T, which can be derived from mass, momentum and energy balances

$$\frac{\partial V}{\partial t} + V\frac{\partial V}{\partial x} + \frac{1}{\rho}\frac{\partial p}{\partial x} = \frac{1}{\rho}\left[\Lambda_V - V\Lambda_\rho\right], \tag{1a}$$

$$\frac{\partial p}{\partial t} + \rho c^2\frac{\partial V}{\partial x} + V\frac{\partial p}{\partial x} + \rho c^2\frac{V}{A}\frac{\partial A}{\partial x} = \phi\left[\Lambda_e - V\Lambda_V - \left(w - \frac{V^2}{2} - \frac{c^2}{\phi}\right)\Lambda_\rho\right], \tag{1b}$$

$$\frac{\partial T}{\partial t} + \phi T\frac{\partial V}{\partial x} + V\frac{\partial T}{\partial x} + \phi T\frac{V}{A}\frac{\partial A}{\partial x} = \frac{1}{\rho c_v}\left[\Lambda_e - V\Lambda_V - \left(w - \frac{V^2}{2} - \phi c_v T\right)\Lambda_\rho\right]. \tag{1c}$$

In Eqs. (1a)–(1c), see nomenclature, A is the flow cross-section (with slow variations along the conductor explicitly accounted for [17]). The convective coupling through the perforated fraction of the helical interface between the two regions is driven by the pressure difference between hole and bundle, while the conductive coupling is driven by the temperature difference.

The strands and the jacket are separately modeled by the one-dimensional heat conduction equation (the heat capacity of and the thermal conduction along the helix are neglected). Jacket and strands are thermally coupled, and also with the helium, and they can be heated externally and/or by Joule effect when the conductor quenches. A uniform current distribution is assumed

over the total strand cross-section, and the Joule heat is computed with a simple resistive model.

Linear finite elements are used for the spatial discretization of the final set of equations, with optional upwind stabilization of the convective terms. An adaptive spatial mesh is used to follow the quench fronts. The resulting set of ordinary differential equations in time is linearized by frozen coefficient leading to

$$\frac{\mathrm{d}\underline{u}}{\mathrm{d}t} = \underline{\underline{\ell}}\,\underline{u}, \tag{2}$$

where $\underline{\underline{\ell}}$ is the coefficient matrix and $\underline{u}$ is the vector of unknowns. Implicit time discretization, with adaptive time step, is adopted for the solution of Eq. (2). The column vector $\underline{u}$ is composed by $8 \times NODES$ components, where "$NODES$" represents the number of nodes in the spatial mesh and 8 is the number of unknowns in each node. Thus, for node n, the vector $\underline{u}$ contains the unknowns

$$\underline{u}((n-1)\times 8+1,\ldots,n\times 8) = [V_{\mathrm{H}}(n)\ V_{\mathrm{B}}(n)\ p_{\mathrm{H}}(n)\ p_{\mathrm{B}}(n)\ T_{\mathrm{H}}(n)\ T_{\mathrm{B}}(n)\ T_{\mathrm{St}}(n)\ T_{\mathrm{Jk}}(n)]^{-1}, \tag{3}$$

where $V(n)$, $p(n)$ and $T(n)$ are the hole (subscript H) and bundle (subscript B) computed values of flow speed, pressure and temperature, respectively, while $T_{\mathrm{St}}(n)$ and $T_{\mathrm{Jk}}(n)$ are the computed values of strand and jacket temperature, respectively, always in node n.

Boundary conditions for the fluid equations are imposed following the theory of characteristics, while adiabatic conditions are assumed at the conductor ends for strands and jacket [1].

The resulting set of equations is solved at each time step by a banded-system solver, with a computational cost proportional to the number of unknowns.

The model implemented in Mithrandir has been validated against quench and heat slug data of QUELL, both with [16] and without [18–20] the simultaneous simulation of the external circuit using Flower [14,15] showing good to very good agreement with the experimental data. More recently, the capability of the code to accurately describe thermal-hydraulic transients in a more complex joint + conductor system has been proven [17].

2.2. Description of the multi-conductor model in M&M

The main limitation to the use of the Mithrandir code as predictive tool for some superconducting systems is that the detailed analysis of only one conductor is allowed by the coupling with the hydraulic network simulator. Several real systems, however, need the simultaneous analysis of more than one conductor, because the coupling between them may not be negligible and/or their approximation as a heated pipe may be insufficient.

The M&M code has been developed from Mithrandir in order to provide a simultaneous description of an arbitrary number $NCOND$ of one- or two-channel CICCs, each one treated in a Mithrandir-like fashion. Each conductor is defined by a separate set of geometrical and material properties, magnetic field and external heating. The spatial discretization accounts for different (adaptive) meshes on different conductors.

The set of equations solved by M&M is

$$\frac{\mathrm{d}\underline{U}}{\mathrm{d}t} = \underline{\underline{L}}\,\underline{U} + \underline{\underline{K}}. \tag{4}$$

In Eq. (4), the unknown vector $\underline{U}$ is defined as

$$\underline{U} = \begin{bmatrix} \underline{u}_1 \\ \underline{u}_2 \\ \cdots \\ \underline{u}_{NCOND} \end{bmatrix}, \tag{5}$$

where $\underline{u}_i$ is the unknown vector for the ith conductor, as defined in Eq. (3). The block diagonal matrix $\underline{\underline{L}}$ is defined as

$$\underline{\underline{L}} = \begin{bmatrix} \left(\underline{\underline{\ell}}_1\right) & 0 & \ldots & 0 \\ 0 & \left(\underline{\underline{\ell}}_2\right) & 0 & \ldots \\ \ldots & 0 & \ldots & 0 \\ 0 & \ldots & 0 & \left(\underline{\underline{\ell}}_{NCOND}\right) \end{bmatrix}, \tag{6}$$

where $\underline{\underline{\ell}}_i$ is the coefficient matrix for the ith conductor, as in Eq. (2). The coupling matrix $\underline{\underline{K}}$ contains the off-diagonals terms, due to the coupling between different conductors in the direction *perpendicular* to that of the flow, which are related to temperature and/or pressure differences between conductors

$$\underline{\underline{K}} = \begin{bmatrix} 0 & K_{1\leftrightarrow 2} & \ldots & K_{1\leftrightarrow NCOND} \\ K_{2\leftrightarrow 1} & 0 & K_{2\leftrightarrow 3} & \ldots \\ \ldots & \ldots & \ldots & K_{(NCOND-1)\leftrightarrow NCOND} \\ K_{NCOND\leftrightarrow 1} & \ldots & K_{NCOND\leftrightarrow (NCOND-1)} & 0 \end{bmatrix}, \tag{7}$$

where block $K_{i\leftrightarrow j}$ accounts for the coupling between the ith and the jth conductor.

In Eq. (7), the elements of block $K_{i\leftrightarrow j}$ are defined in terms of $k_{i\leftrightarrow j}(x_1^i, x_2^j)$, which gives the coupling fluxes between the point located at position x_1 on the ith conductor and the point located at position x_2 on the jth conductor (both coordinates being measured from the respective conductor inlet). $k_{i\leftrightarrow j}(x_1^i, x_2^j)$ is defined as

$$k_{i\leftrightarrow j}(x_1^i, x_2^j) = S_{i\leftrightarrow j}(x_1^i, x_2^j) \times D_{i\leftrightarrow j}(x_1^i, x_2^j) \times C_{i\leftrightarrow j}(x_1^i, x_2^j), \tag{8}$$

where $S_{i\leftrightarrow j}(x_1^i, x_2^j)$ is the exchange perimeter, $D_{i\leftrightarrow j}(x_1^i, x_2^j)$ is the driving term for the coupling between x_1^i and x_2^j

Table 1
Coupled components and driving terms of different kinds of coupling implemented in the M&M code, between the generic ith and jth conductors

Coupling type	Exchanged property	Component involved in the coupling		$D_{i\leftrightarrow j}(x_i, x_j)$
		ith conductor	jth conductor	
Ω_1	Mass	He_B	He_B	Δp
	Momentum	He_B	He_B	Δp
	Energy	He_B	He_B	Δp
	Energy	He_B	He_B	ΔT
	Energy	He_B	Jacket	ΔT
Ω_2	Energy	Jacket	Jacket	ΔT

(i.e., pressure difference Δp or temperature difference ΔT, see Table 1) and $C_{i\leftrightarrow j}(x_1^i, x_2^j)$ is the transport coefficient in the exchange between the two conductors. (If, for example, the exchanged property between ith and jth conductor is energy, then $D_{i\leftrightarrow j}(x_1^i, x_2^j) = [T^i(x_1^i) - T^j(x_2^j)]$ and $C_{i\leftrightarrow j}(x_1^i, x_2^j) = h(x_1^i, x_2^j)$, where h is the heat transfer coefficient.)

The choice of the reference frames on the ith and jth conductors, for the identification of x_1^i, x_2^j, respectively, can account for different topologies of the coupling. Consider, for example, two identical conductors, which are coupled along the whole length x_L. "Co-current" coupling (i.e., with helium flowing in the same direction in both conductors as, e.g., in the SS-FSJS [6,17]) can be reproduced considering the same reference frame in both conductors. "Counter-current" coupling (as, e.g., in the TFMC full size joint sample [7]) can be reproduced using the mapping $x_2^j = (x_L - x_1^i)$. More complicated topologies (as, e.g., in the CSMC inner and outer module) can also be modeled.

In principle, any kind of thermal-hydraulic coupling between conductors, as defined in Eq. (7), can be implemented in M&M, using the form given in Eq. (8). At present, the available choices are (see Table 1),

- Coupling Ω_1, including mass, momentum and energy exchanges. These are implemented with a rough valve model, as that used in Mithrandir for the hole-bundle coupling in a single two-channel conductor, see [1]. This coupling can be used, e.g., to simulate sub-channels, or a single two-channel CICC.
- Coupling Ω_2, including heat exchange between the jackets of adjacent conductors, driven by the temperature difference between the two solids. This accounts for the thermal resistance of the material interposed between the two jackets (e.g., the insulation in the CSMC conductors or the copper sole in the lap joints).

In order to compute, from the generic $k_{i\leftrightarrow j}(x_1^i, x_2^j)$, the elements of the block $K_{i\leftrightarrow j}$ of the coupling matrix $\underline{\underline{K}}$, the axial coordinates corresponding to the spatial nodes of the ith conductor must be considered. For each value of x_1^i, the value of x_2^j coupled to it is determined. Consider, for the sake of simplicity, x_2^j as the axial coordinate of a certain node on the jth conductor. Two coupled nodes on the ith and jth conductor, respectively, are found. With this information, the exact row and column of $K_{i\leftrightarrow j}$, where $k_{i\leftrightarrow j}$ should be put depends only on which components are coupled (e.g., helium bundle or jacket), once a certain order of the unknowns in each node has been chosen (see Eq. (3)).

2.3. Implementation of the multi-conductor model in M&M

We want to solve Eq. (4) with the same efficient banded-system solver used in Mithrandir. This depends on the choice of time-discretization, in particular on the implicit or explicit treatment of the matrix $\underline{\underline{K}}$. Indeed, an implicit treatment of $\underline{\underline{K}}$ would destroy the banded structure, leading to a system that can be solved only with a significant increase of computational cost and CPU time. An explicit treatment of the matrix $\underline{\underline{K}}$, on the contrary, maintains the banded-structure of the coefficient matrix and will be adopted here (computational cost proportional now to $\sum_{1\leqslant i\leqslant NCOND} 8 \times NODES(i)$). There are several additional advantages in this strategy: (1) if the elements of $\underline{\underline{K}}$ are computed explicitly, then the blocks in matrix $\underline{\underline{L}}$ are de-coupled, so that the solution can be computed sequentially for the different blocks, i.e., for the different conductors. (2) The basic structure of Mithrandir can be used, unchanged, as core of M&M. (3) The solution of Eq. (4) sequentially for each conductor leads also to smaller memory occupation with respect to the solution of the banded system as a whole. On the other hand, of course, the explicit treatment will be paid by a typically lower maximum time step, than could be affordable with an implicit method.

The flow chart of the solution algorithm used in M&M is reported in Fig. 2. A common time step Δt for all conductors is chosen for time marching. Δt is chosen to be the smallest between the time steps computed separately for each conductor. At each time step from t to $t + \Delta t$, iterations can be necessary to accurately compute the solution. If m is the iteration index, at the mth iteration the coupling terms for all conductors are computed using the solution $\underline{U}_{m-1}^{t+\Delta t}$ computed at the previous iteration, and for each conductor the respective system (see above) is solved. The global error ε in the solution at iteration m is defined as the maximum over all conductors and all different variables y (pressures and temperatures only) of $\sum_i (y_i{}^m - y_i{}^{m-1})^2 / \sum_i (y_i{}^m)^2$, where i runs over the nodes. If the needed relative accuracy TOL is not reached (i.e., if $\varepsilon > TOL$), at least another iteration is needed. The iterations are under-relaxed, i.e., $\underline{U}_m^{t+\Delta t}$ is linearly combined with $\underline{U}_{m-1}^{t+\Delta t}$ to obtain the actual $\underline{U}_m^{t+\Delta t}$,

$$\underline{U}_m^{t+\Delta t} = \alpha \times \underline{U}_m^{t+\Delta t} + (1-\alpha) \times \underline{U}_{m-1}^{t+\Delta t}, \tag{9}$$

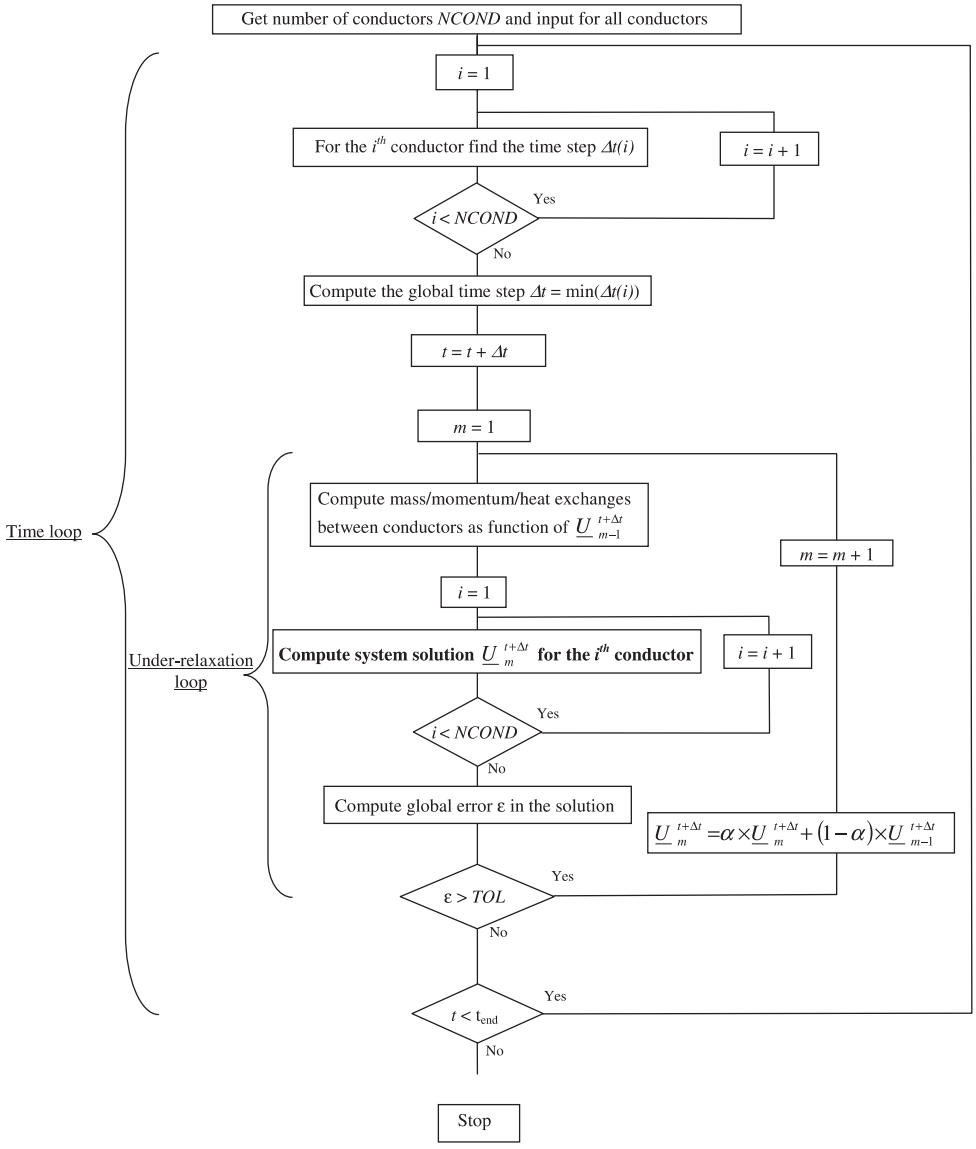

Fig. 2. Flow-chart of the solution algorithm used in the M&M code.

which will be used in the next iteration (α is an appropriate under-relaxation coefficient, with $0 \leqslant \alpha \leqslant 1$).

Boundary conditions can be imposed separately at the ends of each conductor, in the case when they are not hydraulically connected in a network. Otherwise, the coupling of the M&M code with the hydraulic network solver Flower [14,15] provides self-consistent boundary conditions to all the conductors, so that complex systems with conductors hydraulically in parallel and/or in series can be simulated.

The hydraulic series of *NCOND* conductors could be reproduced also without a network solver, by an appropriate sorting of the conductors in the solution time loop (see Fig. 2), based on the above-mentioned splitting of Eq. (4) in *NCOND* de-coupled systems. To simulate a generic series of two conductors, the upstream conductor needs to be solved first, imposing the inlet mass flow rate, pressure and temperature. The computed outlet pressure and temperature and mass flow rate of the first conductor provide the inlet conditions for the downstream conductor, which can then be solved.

3. Code validation

The M&M code has been applied first to an artificial quench in the QUELL conductor, then to a case of heat exchange among different petals in a CSMC-like conductor, and finally to heat exchange in the SS-FSJS. In the first case, a comparison is made with the results

obtained with Mithrandir, while in the other cases a comparison with experimental data is presented.

3.1. Artificial quench in QUELL

We model the single dual-channel conductor of QUELL as *two* coupled conductors. Conductor #1 accounts for bundle helium + jacket + strands of the actual conductor, while conductor #2 simulates the central channel. The central helix is modeled as the jacket of conductor #2. (As a difference with respect to the single-conductor model, the thermal capacity and conductivity of the helix are therefore taken into account here.) Coupling Ω_1 (see Table 1 and above) is present between the two conductors. Each point on the first conductor is coupled with the point having the same axial position on the second conductor (as in the co-current coupling discussed before). The length of the conductor, the material properties and the field distribution along the conductor are the same as in the QUELL experiment.

A short and, as such, artificial quench transient has been simulated with this setup, as a sort of global check of the M&M architecture and of the capability to reproduce strong coupling between conductors. A constant power $Q_0 = 5000$ W/m is deposited over 2.3 m around the center of the conductor length (40.929 m $\leqslant x \leqslant$ 43.229 m), directly into the strands of conductor #1, where a constant transport current $I = 8$ kA is present. Constant p_{in}, p_{out} and T_{in} are imposed at the ends of the conductor. The transient evolution is studied for 5 ms. In Fig. 3, the computed spatial profiles at $t = 2.5$ ms have been reported, while the quench starts after $\sim$1 ms (not shown). The results obtained with Mithrandir, which is, as seen above, a validated tool for quench transients, are also reported in Fig. 3 for the sake of comparison.

One can notice the helium pressurization under the heated zone, due to external + Joule heating (Fig. 3(a)). The coupling between hole and bundle through the helical interface leads to pressure relief in the hole, so that $p_B \approx p_H$. Spikes in the flow speed mark the two propagating fronts (Fig. 3(c)) of the pressure wave, where steep gradients are present. Two quenched regions are growing (not shown) in the heated zone, around the position where the magnetic field reaches its maxima [18]. Since this transient is very fast compared to the

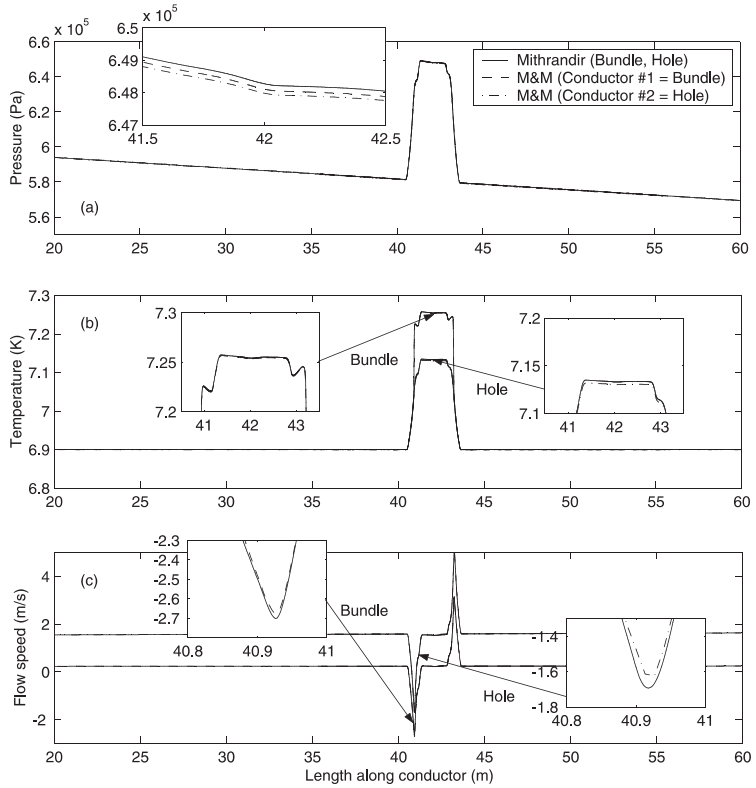

Fig. 3. Artificial quench of the QUELL conductor. Spatial profiles of the solution at $t = 2.5$ ms. The solid lines represent the solution computed with Mithrandir, the dashed and dash-dotted lines the solution computed with M&M (conductor #1 and #2, respectively). (a) Helium pressure; the inset represents a zoom of the pressure in the quenched region. (b) Bundle helium and hole helium temperature. The left inset represents a zoom of the bundle helium temperature in the quenched region; the right inset represents a zoom of the hole helium temperature in the quenched region. (c) Bundle helium and hole helium flow speed. The left inset represents a zoom of the bundle helium flow speed at the left edge of the quenched region; the right inset represents a zoom of the hole helium flow speed at the left edge of the quenched region.

heat exchange time scale between bundle and hole, a significant de-coupling between T_B, and T_H can be noticed in Fig. 3(b).

Overall, a very good agreement between the solutions computed with M&M and Mithrandir is obtained. Minute differences can be seen in the heated region (see insets). However, since the model implemented in the M&M code with $NCOND = 2$ is not fully coincident with the one implemented in Mithrandir (see above), some difference is expected in the results. Notice, however, that the small difference confirms the accuracy of the traditional approximation [18], where thermal capacity and conductivity of the helix are neglected.

An additional aspect of this first simulation is worth mentioning, and it concerns the present model limitation due to the explicit implementation of the coupling between conductors. Obviously, the explicit recipe is cheap from the point of view of CPU time (i.e., it allows relatively big time steps) only when the coupling terms are not too strong, while it requires smaller and smaller time steps as the coupling increases. In this case, in view of the very strong coupling between the two conductors, a very small threshold TOL in the under-relaxation loop is necessary (see Fig. (2)). Alternatively, very small time steps ($\Delta t \sim 10^{-5}$ s) must be used in order to get a stable solution. This explains why only a very short transient of this type has been simulated here.

3.2. Heat exchange between petals in a CSMC-like conductor

In both CSMC and TFMC conductors, a thin (~0.1 mm) Inconel wrapping is applied to the last-but-one stage of the conductor cabling in order to reduce the coupling losses in the cable. The wrapping, with nominal coverage of about 90%, forms six sub-channels, which constitute partially de-coupled parallel paths for the helium flowing in the cable (see Fig. 1(b)). If a resistive heater, short with respect to the strand pitch, is located on the jacket of the conductor, and its width is small compared to the cable external perimeter, the ohmic heat will be deposited mainly in one petal, the others remaining approximately unperturbed. The cross-section of the conductor under the heater, thus, is not isothermal, and, because of the finite time scale of the thermal coupling between the helium in two adjacent petals (O(10s)), isothermal conditions in the conductor cross-section may be found typically only some pitch lengths downstream of the heater (the time scale for helium convection along half pitch length being O(1s)). The experimental evidence of this phenomenon is shown in [21], where a significant non-uniformity between opposite petals is shown half a pitch length downstream of a resistive heater in a CSMC-like conductor. In the experiment, the central channel was blocked, to enhance the effect of inter-petal heat exchange.

We want to reproduce with M&M, at least qualitatively, the above-mentioned experimental result. The six petals of the CSMC-like conductor have been modeled as six different conductors without central channel (see Fig. 1), embedded in a very thin jacket (the wrapping). $NCOND = 7$ is needed to properly model the actual conductor, since an additional conductor beside the petals accounts for the actual Incoloy jacket and for the bundle helium contained in the corners between petals and jacket. A combination of coupling $\Omega_1 + \Omega_2$ has been considered between the different conductors as shown in Fig. 1(b). Each petal can thus exchange with the two adjacent petals mass, momentum and energy through the perforated fraction of the wrapping, and again energy through the contact between the wrappings (i.e., between the Inconel "jackets"). All petals are also coupled with the Incoloy jacket and with the bundle helium in the corners. For the sake of simplicity, the contact perimeter $S_{i\leftrightarrow j}(x_1^i, x_1^j)$ between petals, and between petal and Incoloy jacket, is supposed to be the same (i.e., ~1/3 of the total wrapping perimeter around a single petal, since the central channel is neglected here as seen above). For the heat exchange through the jacket of the petals, $C_{i\leftrightarrow j}(x_1^i, x_1^j)) = h = 2\times$(conductivity/thickness) of the wrapping; the contact thermal resistance between two wrappings has been neglected.

The same geometrical and material properties as in [21] have been used in the M&M simulation. A total helium mass flow rate of 6.6 g/s is given, with inlet pressure $p_{in} \sim 9.5$ bar. Three different input powers ($Q = 2.8$, 4.7 and 6.3 W, respectively [21]) are supposed to be deposited directly into the strands of the first petal (conductor #1) over a length of 0.05 m. This is only a rough approximation of the real situation, where the heat is deposited first into the Incoloy jacket.

The steady-state temperature increase computed in the heated petal (conductor #1) and in the petal on the opposite side of the central channel (conductor #4), at the same axial location 0.250 m downstream of the heater, are reported in Table 2. The experimental data [21] are also reported for the sake of comparison. As seen above, the helium flows in each petal somewhat decoupled from the rest of the conductor, due to the presence of the wrapping. Since only one petal is heated, conductor #1 in Fig. 1(b), say, heat will be exchanged between conductor #1 and conductors #2 and #6 only in a finite time (i.e., on a finite length), and even more slowly between these and conductors #3 and #5. The farthest petal, conductor #4, receives, on a length comparable to the petal pitch, only a small amount of the input power. This explains the non-uniformity observed on the overall conductor cross-section, when the temperature sensors are sufficiently close to the heater.

As expected, also in the simulation the steady-state temperature increase in conductor #4 is much smaller than that in conductor #1. A qualitative agreement is

Table 2
Comparison of computed (M&M) and experimental values of steady state temperature increase (with respect to the inlet value) in heated and non-heated petals of a CSMC-like conductor, 0.250 m downstream from the heater, for different heating power Q

	$Q = 2.8$ W		$Q = 4.7$ W		$Q = 6.3$ W	
	M&M	Exp[a]	M&M	Exp[a]	M&M	Exp[a]
ΔT in heated petal #1 (K)	0.27	0.23–0.25	0.45	0.39–0.41	0.59	0.53–0.55
ΔT in non-heated petal #4 (K)	0.09	0.02–0.04	0.14	0.04–0.06	0.19	0.05–0.06

[a] The experimental values are extracted from Fig. 5 in [21]. The accuracy of the temperature measurements in 21 is ~0.01 K (P. Bruzzone, Private communication, 2000).

obtained between the computed and the experimental ΔT. The agreement is also (probably by chance) quantitative for the temperature increase of the heated petal, while the temperature increase of conductor #4 is more significantly overestimated. Many simplifying hypotheses, however, have been made in the modeling of the coupling between the petals (e.g., heating power all in the petal strands, neglect of contact resistances, etc.), and many uncertainties are present (effective perforated fraction of the wrapping, contact perimeters between solids, etc.). This can qualitatively justify the residual discrepancies.

3.3. Heat exchange in the stainless steel full size joint sample

In the case of the SS-FSJS, the M&M code has been used to simulate the heat exchange between the two sample legs, see Fig. 4. The joint region and part of the conductor (~1 m) are taken into account in each leg, as previously done in [17]. Coupling Ω_2 (see Table 1) is present between the two half joints. The 3-D structure of the jacket in the joint region is neglected: the jacket there is modeled as a homogeneous mixture of copper and stainless steel. We model the thermal resistance between the jackets (i.e., between the two half joints) as that coming from heat conduction through the given thickness of copper sole and PbSn soldering (see Fig. 4(b)). $S_{1\leftrightarrow 2}(x_1^1, x_1^2)$ is equal in this case to the (constant) width of the copper sole. The resulting thermal coupling between the joint halves is very strong, leading to $C_{i\leftrightarrow j}(x_1^i, x_2^j) = h \sim 10^4$ W/m^2 K in Eq. (8).

Experimental run #E1217015, with asymmetrical heating, magnetic field ≈ 10 T and no current, has been considered here. In this run, up-and-down heating steps (0 W → 10 W → 30 W → 50 W → 0 W) have been imposed upstream of the right leg, the left leg being heated only by heat exchange through the copper sole. The nominal mass flow rate in both legs is 5 g/s (±0.5 g/s). In the simulation, we impose as boundary conditions in each leg the inlet temperature (taken from the measured LT5 and RT5, respectively, see Fig. 5), the inlet helium flow speed in bundle and hole (computed from the measured mass flow rate at steady state) and the mea-

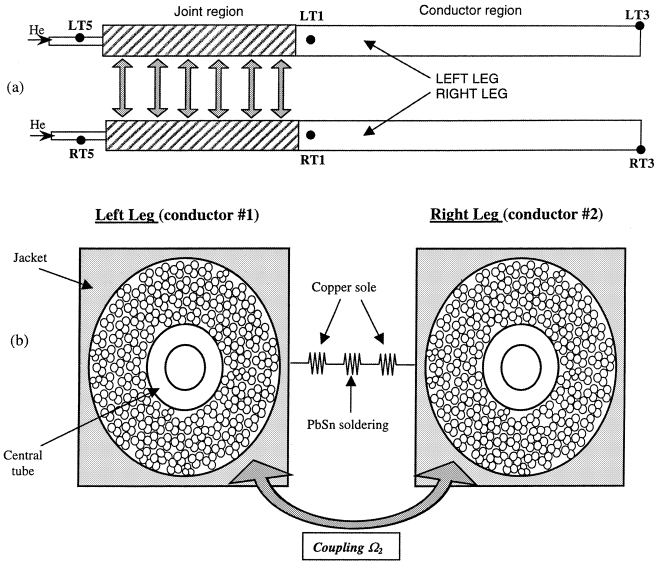

Fig. 4. Schematic view of the joint region in the SS-FSJS experiment, modeled by the M&M code with *NCOND* = 2. (a) Temperature-driven thermal coupling is present only in the joint region of the two legs. Temperature sensors LT5, RT5 are located upstream of the joint inlet, LT1 and RT1 at the joint outlet and LT3, RT3 downstream in the conductor. (b) The heat transfer takes place between the jackets of the two half joints; the heat transfer accounts for the thermal resistance of copper sole and of PbSn soldering.

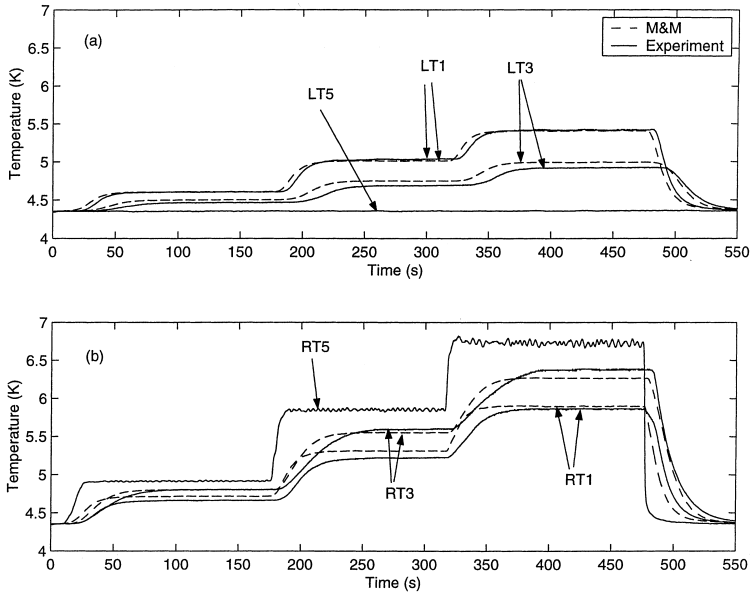

Fig. 5. Analysis of SS-FSJS run #E12017015 (up-and-down steps transient with asymmetrical heating). Time evolution of the temperature at different locations in the left leg (a) and in the (heated) right leg (b) of the sample. The solid lines represent the experimental data; the dashed lines the results computed by the M&M code. In the simulation, LT5 and RT5 are imposed as boundary conditions, while LT1, RT1 and LT3, RT3 result from the computation.

sured p_{out}. In Fig. 5, the computed temperatures at joint outlet and at conductor outlet are compared with the experimental data (signals from LT1, RT1 and LT3, RT3, respectively).

We can notice first that RT1 < RT3, while LT1 > LT3. This happens because RT1 is measured in the bundle just at the outlet of the joint region, and a significant de-coupling between T_B and T_H is present there due to the thick non-perforated central tube separating hole and bundle [6,17]. In the conductor region, on the contrary, the hot helium in the hole is able to heat the bundle helium, and the temperature in RT3 (measured on the jacket, well coupled to the bundle helium) is higher than in RT1, see Fig. 5(b). In the left leg the opposite happens: in the conductor region the cold helium in the hole can cool the bundle helium, heated in the joint region. Thus, in Fig. 5(a) the signal in LT3 is smaller than that in LT1.

A good agreement ($\Delta T \leqslant 0.1$ K) is found between the simulation and the experiment in the plateaus, indicating that the heat exchange between the two legs is well reproduced by our model. The transient portions of the steps, however, are not as well reproduced as the steady state. This is probably due to the fact that the tiny tubes supplying helium to the joint, where the T5 sensors are located, are not included in the simulation.

4. Conclusions and perspective

A novel tool, the M&M code, has been developed from the Mithrandir code, for the simulation of thermal-hydraulic transients in superconducting magnets, made by several one- or two-channel CICCs. The multi-conductor model implemented in M&M has been presented, and the new code has been validated. Comparison is made with Mithrandir results in one case and with experimental data in two other situations, both characterized by strong coupling between the conductors, although of different nature. The response of the M&M code in all cases is good, leading to accurate results.

In perspective we will apply M&M to the analysis of Tcs measurement and quench propagation in the CSMC and TFMC test programs. With suitable modifications, the novel tool should also be applicable and relevant for the thermal-hydraulic analysis of high Tc superconducting power transmission cables [22].

Acknowledgements

The present work has been partially supported by the European Fusion Development Agreement (EFDA) and by the Italian Ministry for University and Scientific and Technological Research (MURST). We also thank P. Bruzzone for a discussion of the sub-channel experiment [21].

References

[1] Zanino R, De Palo S, Bottura L. A two-fluid code for the thermohydraulic transient analysis of CICC superconducting magnets. J Fus Energy 1995;14:25.

[2] Luongo CA, et al. Quench initiation and propagation study (QUIPS) for the SMES-CICC. Cryogenics 1994;34(ICEC Suppl.):611.
[3] Anghel A, et al. The quench experiment on long length (QUELL), Final Report, 1997.
[4] Ciazynski D, Schild T, Martinez A. SS-FSJS test in SULTAN, Test results and analysis. CEA Report DRFC/STEP NT/EM 99/15, April 1999.
[5] Michael PC, Gung CY, Jayakumar R, Minervini JV, Martovetsky N. Qualification of joints for the inner module of the xITER CS model coil. IEEE Trans Appl Supercond 1999;9:201.
[6] Savoldi L, Zanino R. Thermal-hydraulic tests on the SS-FSJS experiment, Politecnico di Torino report PT-DE 513/IN, September 1999.
[7] Savoldi L, Zanino R. Thermal-hydraulic tests on the TFMC-FSJS experiment, Politecnico di Torino report PT-DE 514/IN, October 1999.
[8] Mitchell N, et al. ITER CS model coil project. ICEC16 Proceedings, 1996:763.
[9] Tsuji H, et al. ITER central solenoid model coil test program. Presented at the 17th IAEA Fusion Energy Conference, 1998.
[10] Salpietro E. ITER toroidal field model coil (TFMC) design and construction. Fus Technol 1998;34:797.
[11] Komarek P, Salpietro E. The test facility for the ITER TF model coil. Fus Eng Des 1998;41:213.
[12] Zanino R, Bottura L, Rosso C, Savoldi L. Mithrandir+: a two-channel model for thermal-hydraulic analysis of cable-in-conduit super-conductors cooled with helium I or II. Cryogenics 1998;38:525.
[13] Bottura L. A numerical model for the simulation of quench in the ITER magnets. J Comput Phys 1996;125:26.
[14] Marinucci C, Bottura L. The hydraulic solver flower and its validation against the QUELL experiment in SULTAN. IEEE Trans Appl Supercond 1999;9:616.
[15] Bottura L, Rosso C. Hydraulic network simulator model, Internal Cryosoft Note, CRYO/97/004, 1997.
[16] Savoldi L, Bottura L, Zanino R. Simulations of thermal-hydraulic transients in two-channel CICC with self-consistent boundary conditions. Adv Cryo Eng 2000;45:697.
[17] Zanino R, Santagati P, Savoldi L, Marinucci C. Joint + conductor thermal-hydraulic experiment and analysis on the full size joint sample using MITHRANDIR 2.1. IEEE Trans Appl Supercond 2000;10:1110.
[18] Zanino R, Bottura L, Marinucci C. Computer simulation of quench propagation in QUELL. Adv Cryo Eng 1998;43:181.
[19] Zanino R, Marinucci C. Heat slug propagation in QUELL. Part I: experimental setup and 1-fluid GANDALF analysis. Cryogenics 1999a;39:585.
[20] Zanino R, Marinucci C. Heat slug propagation in QUELL. Part II: 2-fluid MITHRANDIR analysis. Cryogenics 1999b;39:595.
[21] Bruzzone P, Fuchs AM, Vecsey G, Zapretilina E. Test results for the high field conductor of the ITER central solenoid model coil. Adv Cryo Eng 2000;45:729.
[22] Moore T. Powering up superconducting cable. EPRI Journal, Spring 1999:10.